

# Autotuning Technique for the Cost Function Weight Factors in Model Predictive Control for Power Electronic Interfaces

Mohammad B. Shadmand<sup>1</sup>, Member, IEEE, Sarthak Jain<sup>2</sup>, Student Member, IEEE,  
and Robert S. Balog<sup>3</sup>, Senior Member, IEEE

**Abstract**—This paper presents an autotuning technique for the online selection of the cost function weight factors in model predictive control (MPC). The weight factors in the cost function with multiple control objectives directly affect the performance and robustness of the MPC. The proposed method in this paper determines the optimum weight factors of the cost function for each sampling time; the optimization of the weight factors is done based on the prediction of the absolute tracking error of the control objectives and the corresponding constraints. The proposed method eliminates the need of the trial-and-error approach to determine a fixed weight factor in the cost function. The application considered is a capacitor-less static synchronous compensator based on the MPC of a direct matrix converter. This technique compensates lagging power factor loads using inductive energy storage elements instead of electrolytic capacitors. The result demonstrates that the proposed autotuning approach of cost function weights makes the control algorithm robust to parameter variation and other uncertainties in the system. The proposed capacitor-less reactive power compensator based on the autotuned MPC cost function weight factor is verified experimentally.

**Index Terms**—Autotuned weight factors, capacitor-less static synchronous compensator (STATCOM), model predictive control (MPC), reactive power compensation.

## I. INTRODUCTION

THE application of model predictive control (MPC) to power electronic converters dates back to the 1980s for high-power applications, but with low switching frequency due to slow speed processors which limits the control loop frequency [1], [2]. Due to this limitation, widespread adoption of MPC was not feasible and practical at that time. Past decade saw the massive improvements in high-speed microprocessors which renewed the interest in the application of MPC to power electronics requiring higher switching frequencies [3]–[6].

Manuscript received February 25, 2018; revised May 3, 2018; accepted June 9, 2018. Date of publication July 27, 2018; date of current version May 1, 2019. This publication was made possible by NPRP grant# 9-204-2-103 from the Qatar National Research Fund (a member of Qatar Foundation). The statements made herein are solely the responsibility of the authors. Recommended for publication by Associate Editor Xu She. (Corresponding author: Mohammad B. Shadmand.)

M. B. Shadmand is with the Department of Electrical and Computer Engineering, Kansas State University, Manhattan, KS 66506 USA (e-mail: mohamadshadmand@gmail.com).

S. Jain and R. S. Balog are with the Department of Electrical and Computer Engineering, Texas A&M University, College Station, TX 77843 USA (e-mail: jainsarthak2091@gmail.com; robert.balog@ieee.org).

Color versions of one or more of the figures in this paper are available online at <http://ieeexplore.ieee.org>.

Digital Object Identifier 10.1109/JESTPE.2018.2849738

One of the main advantages of MPC over the conventional multiloop controllers is its ability to include several control variables with different characteristics such as voltage, current, torque, and switching frequency into a single cost function or single loop which eliminates the designing and tuning of nested loops [7], [8].

Weight factors in the cost function can accommodate different units and scales as well as allow the prioritization of specific control variable over others by appropriately choosing the ratio of the weight factors of the variables. However, selection of these weight factors is not straightforward [2] and requires trial-and-error approximation. Several empirical approaches to determine a fixed weight factor using trial and error have been investigated in [9]. However, a fixed weight factor is not robust to parameter variation and other uncertainties of the system [10].

One of the major challenges while designing the model predictive controller in the multiobjective control system is to appropriately tune the respective weight factors to achieve the control objectives within the desired performance constraint. This can be cumbersome and even lead to the instability of the whole controller if the weight factors are not chosen properly. Nowadays, autotuning methods for MPC have been under study to decrease the burden of designing the controller and to ensure the robust operation by automatically assigning weight factors. The autotuning of the weight factors in MPC for power electronic converters is a new topic of study; however, few methods on tuning of MPC for application in other fields have been reported in the literature. Garriga and Soroush [11] discussed various tuning methods for MPC in chemical engineering applications. The work proposed in [12] introduced the particle swarm optimization method to tune the MPC. This can be a very computationally heavy approach and limit the high bandwidth requirement of the power electronic converters thus overshadowing one of the main advantages of MPC. Liu and Wang [13] introduced an autotuning method based on the convergence of differential of the objectives and the trust region algorithm to change the controller radius which is defined by the weight factors. The algorithm is not as computationally heavy but becomes very complex as the number of objectives increases and depends on solving the quadratic equations of the model.

This paper presents a technique to select optimal values for the weight factors in the MPC cost function for each

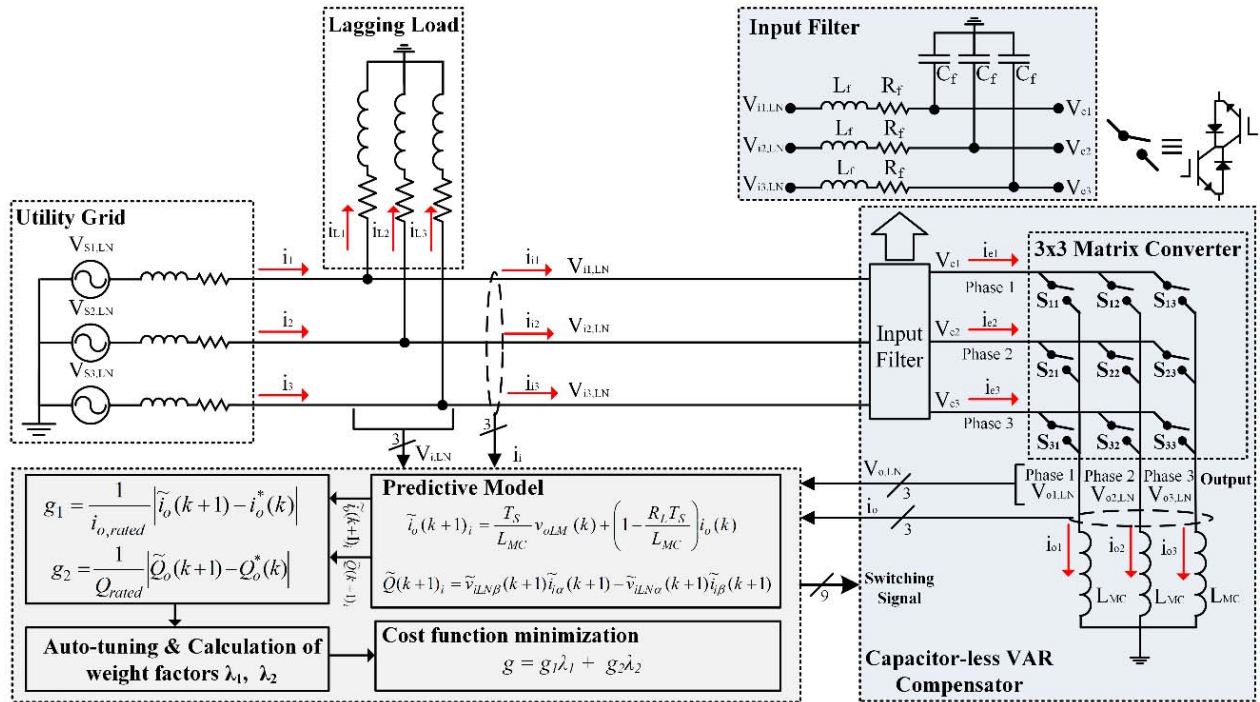


Fig. 1. Capacitor-less VAR compensator employing an MC for the lagging load.

iteration of the MPC loop for power electronic converters. The online optimal selection of the weight factors is robust and is shown to improve the performance of the system when compared to the conventional fixed-value weight factor for MPC. The proposed approach is verified by its application to a capacitor-less static synchronous compensator (STATCOM) technique that uses only inductors combined with an MPC matrix converter (MC) [10], [14].

Reactive power compensation techniques can broadly be classified as passive and active. Passive techniques generally employ large capacitor banks which can be discretely switched individually or in a group to control reactive power. This discrete variation does not allow the precise control of reactive power control and results in over/under compensation in most cases. This can be eliminated by using active methods which employs power electronic interfaces (PEIs) employing semiconductor devices which switches capacitors at high frequency compared to utility to precisely compensate for reactive power among which STATCOM has been widely studied and developed due to its flexible operation [15], [16].

Capacitors are one of the most vulnerable components to fail in power electronic systems [17] and have reliability problems due to their aging characteristics [18]. The associated failure modes including increased leakage currents and other effects from the loss of electrolyte that increases losses and hasten further degradation leading to open-circuit or short-circuit failure modes [19]–[24] with the most frequent failure types listed in [25]. Yet due to the high energy density, low cost, and suitable voltage rating of dc electrolytic capacitors (e-caps), they are widely used in power electronic converters for volt-ampere reactive (VAR) compensation even though approximately 60% of power electronic devices failures are due to the use of aluminum e-caps [26]. The voltage-source inverter-

based STATCOM which uses e-caps is vulnerable to this high-rate failure mode [10]. Thus, to ensure long service life and reliability, capacitors need to be replaced periodically and requires health monitoring equipments/techniques [26]–[28] which adds additional cost and complexity to the system.

The VAR compensation technique in this paper does not employ energy storage capacitors; instead, the topology uses inductors to compensate VAR. Inductors are known to be robust and reliable elements with long service life compared to capacitors, but unlike capacitors, they consume reactive power making it impossible to use them directly as reactive power compensators. The application employed in this paper interfaces a  $3 \times 3$  direct MC (DMC) to the inductor bank, which is controlled by MPC with the autotuning weight factor approach to operate it as STATCOM. The general schematic with the control overview of the proposed system is illustrated in Fig. 1. DMC has a unique property of phase inversion between its input and output ports which can basically reflect the inductor as a capacitor to the grid thus allowing reactive power compensation [29]. By using the property of current phase reversal of DMC, the converter provides leading currents to the ac network while the inductor absorbs lagging current at the output side of the converter. As a result, a STATCOM can be derived without using energy storage e-caps by the MC appropriately controlled by MPC. Also, the proposed solution is more reliable and robust and provides long service life of the system. The main contributions of this paper can be summarized as follows.

- 1) Eliminating the need of the trial-and-error approach to determine a fixed weight factor in the cost function of MPC.
- 2) Development of an MPC approach for PEIs robust to model parameter variation.

- 3) Verification of guaranteed stable operation of the proposed MPC method with autotuned weight factors.
- 4) Performance verification of a STATCOM with long service life by eliminating the need of e-cap energy devices and robust to disturbances in the system by autotuning the weight factors.
- 5) Improvement of the grid-side power quality, i.e., grid current compared to the conventional MPC method with the fixed weight factor method. In particular, for the considered application, model parameter error has lower effect on the performance of the proposed MPC and meets IEEE-519 [30], [31] total harmonic distortion (THD) standards with high disturbance rejection.

## II. PRINCIPLE OF MODEL PREDICTIVE CONTROL

With the rapid advancement of microprocessor technologies in last couple of decades, MPC is becoming more reliable and efficient in power electronic applications [3], [32]–[35]. The main characteristic of MPC is predicting the future behavior of the desired control variables [2], [3] until a specific time in horizon. The predicted control variables will be used to obtain the optimal switching state by minimizing a cost function. The discrete-time model of the control variables will be used for prediction, which can be presented as the state space model as follows [2]:

$$x(k+1) = Ax(k) + Bu(k) \quad (1)$$

$$y(k) = Cx(k). \quad (2)$$

Then, a cost function that takes into consideration the future states, references, and actuations can be defined [2], as a general cost function definition is given by

$$g(x(k), u(k)) = \sum_{\ell=k}^{k+N} \lambda(x(\ell), u(\ell)). \quad (3)$$

The defined cost function  $g$  is the sum of the weighed objective function over the finite horizon of  $N$  time steps. The cost function uses  $x(k)$  and a sequence of manipulated variables as arguments

$$u(k) = [u^T(k) \quad u^T(k+1) \quad \dots \quad u^T(k+N)]^T. \quad (4)$$

The future states and control objectives can be predicted for penalizing in the cost function (3) by using  $x(k)$ , argument given in (4), and the system dynamic model.

The implementation of MPC for power electronic converters is illustrated in Fig. 2. In this block diagram, measured variable  $X_i(k)$ , where  $i \in (1, \dots, n)$  and  $i \in \mathbb{N}$ , is used along with the discrete model of the converter to estimate predictions  $\tilde{Y}_i(k+1) = f(X, t)$  using measured variables for all of the  $P$  possible switching states (plants), where  $P \in \{1 \dots P\}$ . These predictions are then evaluated using a cost function which compares them to the reference values  $Y_i(k)$ , where  $i \in (1, \dots, n)$  and  $i \in \mathbb{N}$  by considering the design constraints. Finally, the optimal actuation  $S$  is selected and applied to the converter. The general form of the cost function  $g$  for reference

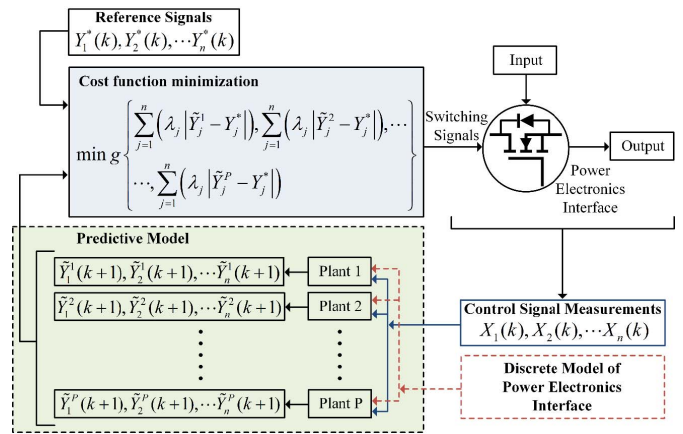


Fig. 2. MPC implementation for power electronic converters.

tracking subject to minimization can be formulated as

$$g = \sum_{j=1}^n (\lambda_j |\tilde{Y}_j^1(k+1) - Y_j^*(k)|) \quad (5)$$

$$\text{s.t. } x(k+1) = Ax(k) + Bu(k)$$

$$y(k) = Cx(k) + Du(k)$$

where  $\lambda_j$  is the value or weight factor for each objective and  $j \in \{1 \dots n\}$  for  $n$  control objectives.

The implementation of the modified MPC algorithm with autotuning of the weight factors of the cost function is illustrated in Fig. 1 and explained in Fig. 4 using flowchart. In the proposed approach, an inner loop is added before the final optimization of the cost function for the purpose of online optimal selection of the weight factors at each sampling time. The cost functions  $g_1, g_2, \dots, g_n$  corresponding to individual objectives of the controller and are converted to a per-unit system. By evaluating the magnitude of these cost functions separately, their weight factors will be optimally selected to meet the predefined constraints. Finally, the general cost function (5) subject to minimization will be constructed. A more detailed explanation of the algorithm for the autotuning approach of the weight factors will be presented in Section IV.

The schematic of the proposed autotuning MPC control is comprehensive and can be applied to any PEI with multiple control objectives. Fig. 3 shows the generalized control diagram of the proposed autotuning MPC for power electronic converter. The block diagram is shown for a power converter with “ $P$ ” plant models each having “ $n$ ” number of objectives to be met by MPC. The error tolerance  $\epsilon$  denotes a small acceptable error in the control objectives and  $\lambda$  denotes the small value of the weight factor which is increased in integral steps as shown in Fig. 4. In this paper, the considered case study is a  $3 \times 3$  DMC and inductive load with STATCOM functionality.

## III. GROUND WORK: PREDICTIVE MODEL FORMULATION OF THE STATCOM

### A. System Description

The VAR compensator system illustrated in Fig. 1 consists of three-phase ac grid, an inductor bank used for compensation, a  $3 \times 3$  DMC, an interface filter between utility and DMC,

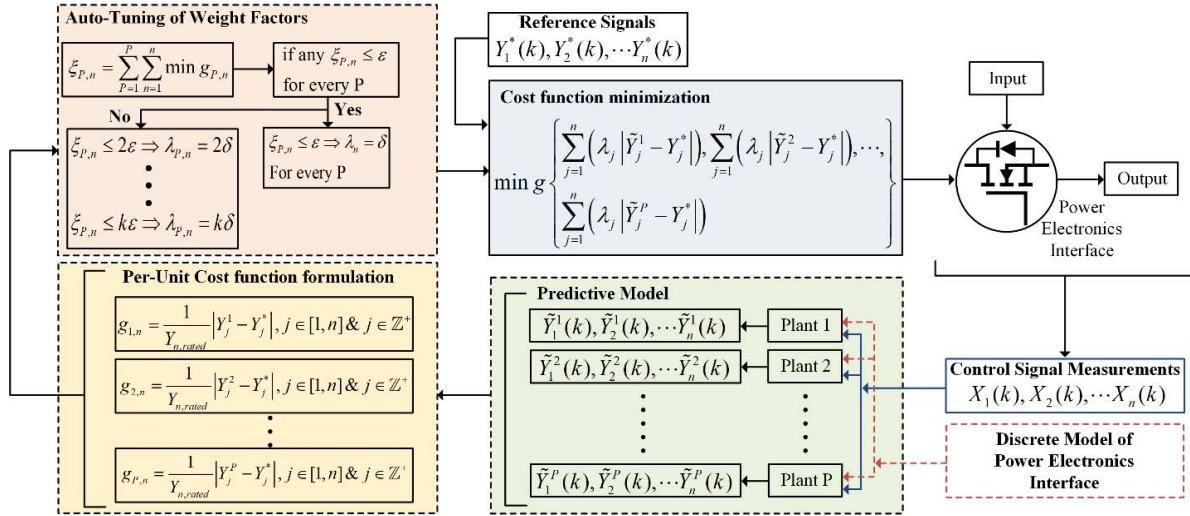


Fig. 3. Overview of the proposed autotuned MPC for power electronic converters.

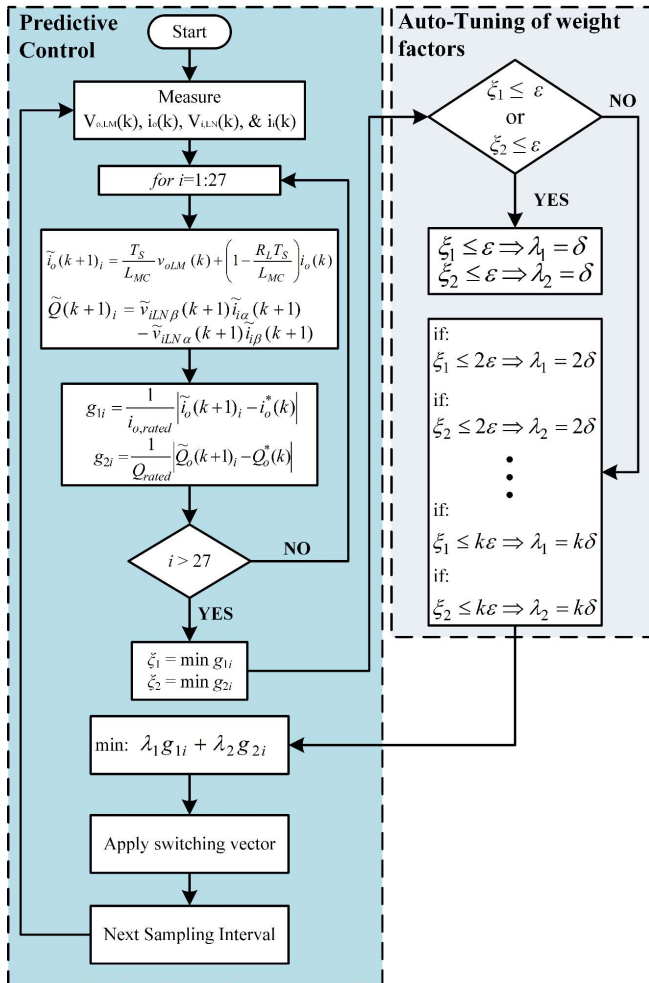


Fig. 4. MPC algorithm of the MC for VAR compensation with dynamic weight factor selection.

and an inductive load as a reactive load to be compensated by DMC-based STATCOM. The reactive power compensator consists of the inductors  $L_{MC}$  connected to the ac network through a  $3 \times 3$  MC. The line-neutral voltages at the point of common coupling (PCC) of the MC are denoted by

$v_{i1,LN}$ ,  $v_{i2,LN}$ , and  $v_{i3,LN}$ , while the output voltages of the DMC are given by  $v_{o1,LM}$ ,  $v_{o2,LM}$ , and  $v_{o3,LM}$ . The currents drawn by the lagging load are denoted by  $i_{L1}$ ,  $i_{L2}$ , and  $i_{L3}$ , while currents drawn by the MC including the filter from the network are  $i_{i1}$ ,  $i_{i2}$ , and  $i_{i3}$ . The currents at the filter–DMC interface are  $i_{e1}$ ,  $i_{e2}$ , and  $i_{e3}$ , while the currents drawn by the choke from the MC are given by  $i_{o1}$ ,  $i_{o2}$ , and  $i_{o3}$ .

The working principle of MC has been explained in detail in [36] and [37] and will not be covered in this paper. Several papers in the literature have investigated the MPC for MCs [3], [38]–[40]. By keeping in mind MC switching scheme restrictions, we can say that the  $3 \times 3$  MC has 27 possible switching states to be considered during the prediction of variables and optimization of the cost function by MPC. In this paper, all possible 27 switching states are considered for evaluating the cost function. These switching states can be classified as follows.

- 1) *Space Vectors With Constant Amplitude and Variable Angle at the Source Angular Frequency*: All output phases connected to different input phases.
- 2) *Stationary Space Vectors With Fixed Direction and Variable Amplitude*: One output phase connected to a different input phase, and the other two output phases connected to the same input phases.
- 3) *Space Vectors With Zero Amplitude*: All output phases connected to the same input phases.

#### B. Current Phase Reversal Property for Matrix Converter

The  $3 \times 3$  DMC topology for VAR compensator is shown in Fig. 1. The detailed proof of the current phase reversal is explained in [10] and is explained here briefly. The DMC can be mathematically modeled using transfer function as

$$\begin{bmatrix} v_{o1,LM} \\ v_{o2,LM} \\ v_{o3,LM} \end{bmatrix} = \mathbf{H} \times \begin{bmatrix} v_{i1,LN} \\ v_{i2,LN} \\ v_{i3,LN} \end{bmatrix}$$

where

$$\mathbf{H} = \mathbf{H}^T = \begin{bmatrix} H_1 & H_2 & H_3 \\ H_2 & H_3 & H_1 \\ H_3 & H_1 & H_2 \end{bmatrix}. \quad (6)$$

$\mathbf{H}$  is known as a modulation matrix or instantaneous transfer matrix. For a lossless system, the instantaneous output and input power of DMC should always be equal. Using Kirchoff's current law, the relationship between input and output currents can be given as

$$\begin{bmatrix} i_{i1} \\ i_{i2} \\ i_{i3} \end{bmatrix} = \mathbf{H}^T \times \begin{bmatrix} i_{o1} \\ i_{o2} \\ i_{o3} \end{bmatrix}. \quad (7)$$

Taking particular modulation function  $\mathbf{H}$  comprised three single-phase functions  $H_1$ ,  $H_2$ , and  $H_3$  from [29] as

$$H_k = \frac{1}{3} \left( 1 + 2 \left( \frac{V_o}{V_i} \right) \cos \left( 2\omega t - \frac{2(k-1)\pi}{3} \right) \right). \quad (8)$$

The line voltage of a three-phase utility can be represented as

$$v_{sk, \text{LN}} = v_{ik, \text{LN}} = \sqrt{2} \times V_{\text{LN, rms}} \cos(\omega t - 2(k-1)\pi/3). \quad (9)$$

Applying  $\mathbf{H}$  matrix from (6) and (8) to compensator in Fig. 1 will result in three-phase MC output voltages can be given by [29]

$$v_{ok, \text{LM}} = \sqrt{2} \times \frac{V_o}{V_i} \times V_{\text{LN, rms}} \cos(\omega t - 2(k-1)\pi/3). \quad (10)$$

For a balanced system, the magnitude of the current for each phase will be identical. Thus, the currents can be represented in the Euler phasor form as follows:

$$\begin{aligned} i_{o1} &= \text{Re}\{\sqrt{2} \times |I_o| \times e^{j(\omega t - \pi/2)}\} \\ &= \text{Re}\{\sqrt{2} \times |I_o| e^{j\omega t} \times e^{-j\pi/2}\} \end{aligned} \quad (11)$$

where  $|I_o| = ((V_o/V_i)) \times (V_{\text{LN, rms}}/\omega L_{\text{MC}})$ , the phasor representation of the output current can be written as

$$I_{o1} = |I_o| \angle -\pi/2. \quad (12)$$

Similarly, input current  $i_{i1}$  can also be expressed as a phasor form as

$$\begin{aligned} i_{i1} &= \text{Re}\{\sqrt{2} \times |I_i| \times e^{j(\omega t + \pi/2)}\} \\ &= \text{Re}\{\sqrt{2} \times |I_i| e^{j\omega t} \times e^{j\pi/2}\} \end{aligned} \quad (13)$$

where  $|I_i| = ((V_o/V_i))^2 \times (V_{\text{LN, rms}}/\omega L_{\text{MC}}) = ((V_o/V_i)) \times |I_o|$ , and input current phasor can be represented by

$$I_{i1} = \left( \frac{V_o}{V_i} \right) |I_o| \angle \pi/2 \quad (14)$$

Thus, from (12) and (14), the MC input current of each phase leads the corresponding output current by  $\pi$ .

### C. Input Filter Modeling

The conventional LC filter is used as shown in Fig. 1 with  $R_f$  as a loss resistance. Input filter is required between MC and ac source to eliminate the high-order harmonics [29], [36], [37]. Input filter may introduce an additional phase shift in voltage, but without loss of generality, it can be assumed that the filter resonances are well damped in properly designed filter and the phase shift will be compensated by the model predictive controller. The detailed modeling of the input filter have been adopted from [10].

For the filter-grid interface, the discrete-time input current is

$$\begin{aligned} i_i(k+1) &= A'(2, 1)V_e(k) + A'(2, 2)i_i(k) \\ &\quad + B'(2, 1)V_{i, \text{LN}}(k) + B'(2, 2)i_e(k) \end{aligned} \quad (15)$$

with coefficients matrices as

$$A' = e^{AT_s}, \quad B' = \int_0^{T_s} e^{A(T_s-\tau)} B d\tau. \quad (16)$$

### D. Controller Design

A load model needs to be obtained in order to predict the value of the load current at the next step sampling interval for all 27 possible switching states. The inductive load at the output side of the MC can be represented as

$$L_{\text{MC}} \frac{di_o(t)}{dt} = v_{o, \text{LM}}(t) - R_L i_o(t) \quad (17)$$

where  $L_{\text{MC}}$  is the inductance and  $R_L$  is the inductor resistance. Using the Euler forward method, the derivative in (17) is approximated using (20) and (21)

$$\frac{di_o(t)}{dt} \approx \frac{i_o(k+1) - i_o(k)}{T_s} \quad (18)$$

$$\tilde{i}_o(k+1) = \frac{T_s}{L_{\text{MC}} + R_L T_s} \left( v_{o, \text{LM}}(k) + \frac{L_{\text{MC}}}{T_s} i_o(k) \right) \quad (19)$$

where  $T_s$  is the sampling period.

Equation (19) estimates the value of the output current of MC for the next sampling interval  $(k+1)$  and the corresponding voltage  $v_{o, \text{LM}}$ , which is calculated for the 27 possible switching states of the MC. Control of reactive power and the output current are the control objectives for the MPC in this paper. The reactive power can be determined by

$$Q(t) = \text{Im}\{v_{i, \text{LN}}(t) \times \tilde{i}_i(t)\} \quad (20)$$

where  $\tilde{i}_i(t)$  is the complex conjugate of  $i_i(t)$ . The current phase reversal property of the MC indicates that  $i_i(t)$  and  $i_o(t)$  are out of phase; thus, the reactive power can be predicted by using

$$\begin{aligned} \tilde{Q}(k+1) &= \text{Im}\{v_{i, \text{LN}}(k+1) \times \tilde{i}_i(k+1)\} \\ &= v_{i, \text{LN}, b}(k+1)i_{i\alpha}(k+1) \\ &\quad - v_{i, \text{LN}, \alpha}(k+1)i_{i\beta}(k+1) \end{aligned} \quad (21)$$

where  $\alpha$  and  $\beta$  correspond to the real and imaginary components of the associated vector. The value of  $v_{i, \text{LN}}(k+1)$  can be approximated to be  $v_{i, \text{LN}}(k)$  because the line voltages are low-frequency signals compared to the switching frequency. By keeping in mind the current phase reversal property of the MC and (19),  $i_i(t)$  can be calculated [14]. The control objectives of the MPC cost function are the input reactive power of the MC (at the PCC of utility grid, load, and DMC) and the current in the inductive load of DMC. The inductive load current is controlled to minimize the THD of the grid current. From (5), (19), and (21), the cost function  $g$  can be formulated as

$$g = \lambda_1 |\tilde{i}_{o, \alpha\beta}(k+1) - i_{o, \alpha\beta}^*| + \lambda_2 |\tilde{Q}(k+1) - Q^*(k)| \quad (22)$$

where the asterisk indicated the reference value and the tilde indicated the predicted value to regulate input reactive power and current into the inductive load.

#### IV. AUTOTUNING OF WEIGHT FACTORS AND STABILITY ANALYSIS

##### A. Autotuning Algorithm

This section presents an autotuning technique for the online selection of the cost function weight factors in MPC. The weight factors in the cost function with multiple control objectives directly affect the performance and robustness of the MPC. The proposed method in this section determines the optimum weight factors of the cost function for each sampling time. The optimum weight factor results in better current quality at the grid side and robustness to disturbances in the model parameters of the system. The optimization of the weight factors is done based on the prediction of the absolute tracking error of the control objectives and the corresponding constraints. Without loss of generality, this technique is applied to the application considered in this paper, a capacitor-less STATCOM technique using MPC of a DMC.

The proposed dynamic weight factor selection of the MPC algorithm for the MC is shown in detail in Fig. 4. After minimization of the cost function  $g$ , the switching that corresponds to the minimum  $g$  will be applied to the converter. Then, the algorithm moves into autotuning of weight factors. The tuned weight factors will be used for the minimization of (22) at the next sampling period for sufficiently small sampling time. In practice, much of the evaluations for tuning of weight factors are based on the computations that have been already done. Thus, using the already computed cost function, we are able to split the cost function (22) into two parts where each corresponds to individual control objectives

$$g_1 = |\tilde{i}_{o,\alpha\beta} - i_{o,\alpha\beta}^*| \leq \Psi_1 \quad (23)$$

$$g_2 = |\tilde{Q} - Q^*| \leq \Psi_2. \quad (24)$$

$\Psi_1$  and  $\Psi_2$  are the acceptable error of tracking commanded values. From the computed  $g_1$  and  $g_2$  for all 27 switching states, the minimum value of  $g_2$  will be selected as

$$\zeta = \min g_2 \quad (25)$$

The next step is to evaluate the magnitude of minimum  $g_2$  with a sufficiently small number  $\varepsilon_1$  as follows:

$$\zeta \leq \varepsilon_1 \Rightarrow \lambda = \varepsilon_2 \quad (26)$$

The statement (26) is presenting that if  $g_2$  is small enough (less than a defined small number  $\varepsilon_1$ ), then the weight factor  $\lambda$  is determined to be equal to a sufficiently small number  $\varepsilon_2$ , considering the fact that  $g_2$  is within an acceptable error range  $\Psi_2$ .

If the condition in (26) is not satisfied, a larger value for weight factor  $\lambda$  should be selected in order to give higher value to  $g_2$  for minimization at the next sampling time ( $k+1$ ). This evaluation of  $\zeta$  when its value is more than  $\varepsilon_1$  is as follows:

$$\zeta \leq 2\varepsilon_1 \Rightarrow \lambda = 2\varepsilon_2$$

$$\zeta \leq 3\varepsilon_1 \Rightarrow \lambda = 3\varepsilon_2$$

⋮

$$\zeta \leq \kappa\varepsilon_1 \Rightarrow \lambda = \kappa\varepsilon_2$$

$$\text{where } \kappa \in \{1, 2, 3, \dots, N\}. \quad (27)$$

The statements in (27) quantized  $\zeta$ , which corresponds to the magnitude of  $g_2$ ; the weight factor  $\lambda$  is determined based on  $\zeta$  magnitude when comparing to  $n$  multiples of  $\varepsilon_1$  till the statement in (27) is satisfied. The corresponding value of  $\lambda$  is multiplication of  $n$  by  $\varepsilon_2$ . This strategy for selecting the weight factor  $\lambda$ , based on the absolute error of  $g_2$  is illustrated in Fig. 4 (right). This procedure will be repeated every sampling time; thus, during every sampling period, the weight factor will be tuned online and applied to the minimization procedure of the cost function (22) at next sampling time.

##### B. Stability Analysis of the System

The system stability is analyzed using the Lyapunov stability criteria. The system is proven to be bounded and shown to asymptotically converge the error function toward zero over the time period. For the presented system, there are 27 switching states which can be applied to the DMC in order to regulate the reactive power. In finite set MPC, the future actual voltage vector  $v_{o,LM}^{\text{opt}}(k+1)$  required for perfect tracking can be represented as

$$v_{o,LM}^{\text{conv}}(k+1) = v_{o,LM}^{\text{conv,opt}}(k+1) + \phi(k+1) \quad (28)$$

where  $v_{o,LM}^{\text{conv}}(k+1)$  shows the converter output voltage vector based on 27 switching states,  $v_{o,LM}^{\text{conv,opt}}(k+1)$  is the optimum voltage vector that can make the current error in the next sampling instant to zero, and  $\phi(k+1)$  represents the quantization error in the voltage vectors; here,  $\|\phi(k+1)\| \leq l$  and  $l \in \mathbb{R}^+$ .

Since  $v_{o,LM}^{\text{conv}}(k+1)$  is bounded and is in finite sets, the hysteresis bounds of  $\phi(k+1)$  are also bounded; thus, the existence of “ $T$ ” is guaranteed. Taking control parameters defined above,  $i_{o\text{-error}}$  can be defined as

$$i_{o\text{-error}}(k+1) = i_o(k+1) - i_{o\text{-ref}}(k+1). \quad (29)$$

From (19)

$$i_{o\text{-error}}(k+1) = \frac{T_S}{L_{MC} + R_L T_S} \left( v_{o,LM}^{\text{conv}}(k) - \frac{L_{MC}}{T_S} i_o(k) \right) - i_{o\text{-ref}}(k). \quad (30)$$

The goal of the control function is to reduce tracking error  $i_{o\text{-error}}$  asymptotically to zero or a very small error tolerance value  $\varepsilon$ .

The Lyapunov function  $L(k)$  is defined as

$$L(i_{o\text{-error}}) = \frac{1}{2} [i_{o\text{-error}}(k)]^T [i_{o\text{-error}}(k)]. \quad (31)$$

Using (31), the rate of change of the Lyapunov function can be defined as

$$\begin{aligned} \Delta L(i_{o\text{-error}}) &= L(i_{o\text{-error}}(k+1)) - L(i_{o\text{-error}}(k)) \\ &= \frac{1}{2} [x]^T [x] - \frac{1}{2} [i_{o\text{-error}}(k)]^T [i_{o\text{-error}}(k)] \end{aligned} \quad (32)$$

where

$$x = \frac{T_S}{L_{MC} + R_L T_S} \left( v_{o,LM}^{\text{conv}}(k) - \frac{L_{MC}}{T_S} i_o(k) \right) - i_{o\text{-ref}}(k+1).$$

According to the Lyapunov theorem, for convergence of  $i_{o\text{-error}}$  and for system to be stable, the rate of change of the

TABLE I  
PARAMETERS FOR THE SYSTEM IN FIG. 1

Parameter	Value
Line-to-neutral grid voltage $V_{LN,rms}$	277.13 V
Angular frequency of grid voltage $\omega$	$2\pi \cdot 50$ rad/s
Per-phase resistance of load $R_{Load, per phase}$	10 $\Omega$
Per-phase inductance of load $L_{Load, per phase}$	30mH
Total rated real power of load $P_{Load}$	2.2 kW
Power factor at the load side $p.f.$	0.9
Total maximum load reactive power requirement $Q_{load}$	2kVAR
MC output-side inductance $L_{MC}$	30mH
Per-phase filter inductance $L_f$	1mH
Per-phase filter capacitance $C_f$	20 $\mu$ F
Sampling time ( $T_s$ )	60 $\mu$ s
Weight factor $\lambda$ of conventional approach	0.008

Lyapunov function  $\Delta L(i_{o-error})$  should be always negative; thus,  $i_{o-error} \rightarrow 0$ , if  $\Delta L(i_{o-error}) < 0$ . To check the above condition, system should follow the following criteria:

$$\begin{aligned}
 L(i_{o-error}(k)) &\geq C_1 |i_{o-error}(k)|^\sigma \quad \forall i_{o-error}(k) \in \Upsilon \\
 L(i_{o-error}(k)) &\geq C_2 |i_{o-error}(k)|^\sigma \quad \forall i_{o-error}(k) \in \Gamma \\
 L(i_{o-error}(k+1)) - L(i_{o-error}(k)) &< -C_3 |i_{o-error}(k)|^\sigma + C_4 \\
 C_1, C_2, C_3, C_4 &\in \mathbb{R}^+, \quad \sigma \geq 1 \quad \Upsilon \in \mathbb{R}^+, \Gamma \subset \Upsilon.
 \end{aligned} \tag{33}$$

From (31) and (32)

$$\Delta L(k) = \frac{1}{2} \left( \frac{T_S}{L} \right) l^2 - \frac{1}{2} [i_{o-error}(k)]^T [i_{o-error}(k)]. \tag{34}$$

Also, the current vector converges to compact set given by

$$\Omega = \left\{ \|i_{o-error}(k)\| \|i_{o-error}(k)\| \leq \frac{T_S}{L} l \right\}. \tag{35}$$

Therefore, all the signals will be bounded and will satisfy the Lyapunov stability criterion.

## V. RESULTS AND DISCUSSION

The system is mathematically modeled and simulated in Simulink–MATLAB. The sampling time ( $T_S$ ) of the MPC is 60  $\mu$ s, the reference reactive power of grid  $Q^*$  is zero VAR [unity power factor (PF)], and other system parameters are given in Table I. A characteristic of MPC is the use of system models for selecting optimal actuations; thus, evaluating the effect of model parameter mismatch on control effectiveness is of interest. The proposed dynamic weight factor selection illustrates that the effect of model parameter errors (sometimes called as model parameter uncertainties) on performance of the system is significantly reduced. In order to demonstrate this fact, the MC output-side inductance ( $L_{MC}$ ) model value is changed from 30 to 15 mH, while the nominal value is 30 mH. The model parameter error is defined as the mismatch between the actual inductor used in the experiment versus the model inductance value in the MPC algorithm.

The simulation results illustrated in Fig. 5 demonstrate the MPC performance of reactive power compensation of MC;

with the conventional fixed weight factor selection based on the trial-and-error tuning method. The optimum weight factor based on the conventional trial-and-error approach is determined as 0.008 [14] and the reference reactive power  $Q^*$  set as zero VAR (unity PF). Fig. 5(a) and (b) demonstrates phase 1 of utility-side voltage and current which are required to be in phase, in addition to the output voltage of MC. At time 60 ms, the mismatch in the inductance at the output side of the MC is applied and its value is dropped to 15 mH from its nominal value (30 mH), as it is shown in Fig. 5(a) and (b). After this parameter variation, the current becomes highly distorted and the STATCOM fails to operate appropriately.

Now by using the proposed autotuning approach of the weight factor of MPC, the distortion can be significantly reduced with inductance model parameter error. The simulation results in Fig. 6 demonstrate this fact. The cost function weight factor is updated instantaneously at each sampling time to achieve real-time autotuning. Phase 1 of the utility voltage and load current are illustrated in Fig. 6(a), and the lagging load PF is illustrated in Fig. 6(b). As it is shown and required for the STATCOM, the grid-side voltage and current are in phase with very small distortion after time 60 ms. Thus, a robust MPC with autotuned cost function weight factors for the objective of capacitor-less STATCOM is achieved. The current phase reversal property is illustrated in Fig. 6(c) which shows the input and output currents of the MC. Phase 1 of output voltage of the MC is illustrated in Fig. 6(d). These results demonstrate negligible distortion in current and voltage waveforms even with this high model error in the output inductance of the MC.

The performance of the proposed autotuned MPC for the considered application is verified experimentally. Fig. 7 shows the experimental setup block diagram used for the analysis of the proposed algorithm. The experimental setup includes a California Instrument MX45 programmable ac power source, dSPACE DS1006 platform to implement the controller, and interface with the MC hardware with nine bidirectional switches. Figs. 8 and 9 illustrate the utility grid voltage, utility grid current, and MC output voltage with the fixed cost function weight factor with and without model parameter errors in the output inductance of MC. The model parameter error is triggered at instant  $t_1$ . As it is captured, the conventional MPC scheme is not robust to model parameter error, and the STATCOM failed to operate appropriately. Figs. 10–12 demonstrate the performance of the proposed autotuning approach of three MPC weight factor. Utility grid voltage, utility grid current, and the output voltage of the MC are shown in Figs. 10 and 11. The reactive power compensation performance, current phase reversal property, and lagging load current are shown in Fig. 12. As it is captured, even after instant  $t_1$  with model parameter error, the STATCOM operates appropriately and continues to compensate the reactive power required by the utility. Thus, the proposed approach improves the robustness of the MPC scheme to model parameter errors in addition to the elimination of “trial-and-error” design process of the weight factor in MPC cost function.

The grid-side reactive power using the proposed autotuned cost function weight factor and the conventional fixed weight

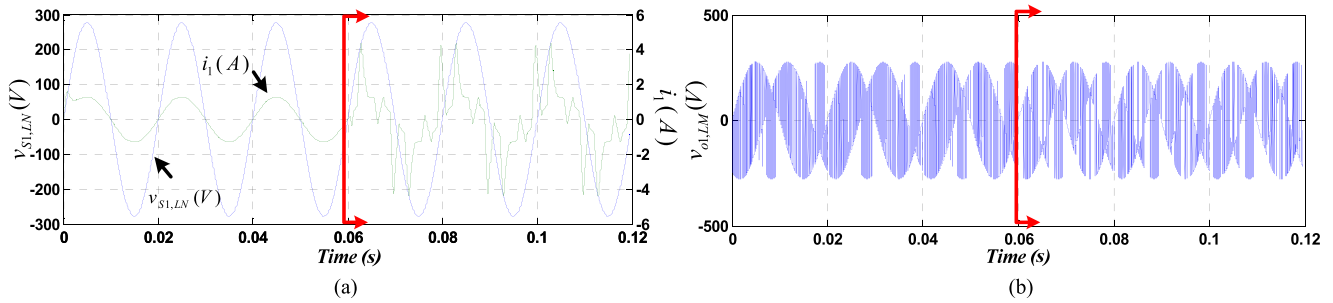


Fig. 5. Simulation results of the conventional fixed weight factor for the MPC cost function for VAR compensation by MC without and with errors in the inductance model at time 0.06 s. (a) Phase 1 of utility power input voltage and current. (b) Phase 1 of output voltage of the MC.

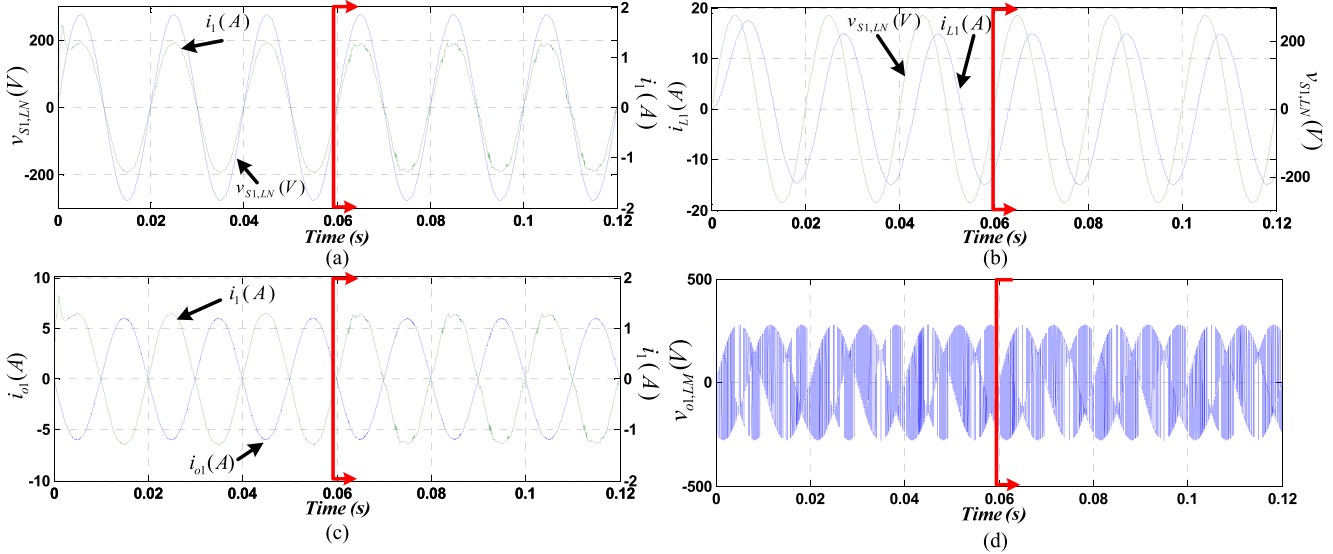


Fig. 6. Simulation results of the proposed autotuning approach of weight factor for the MPC cost function for VAR compensation by MC without and with errors in the inductance model at time 0.06 s. (a) Phase 1 of utility power input voltage and current. (b) Phase 1 of utility voltage and load current. (c) Phase 1 current of the MC shows the phase reversal from input to output. (d) Phase 1 of output voltage of the MC.

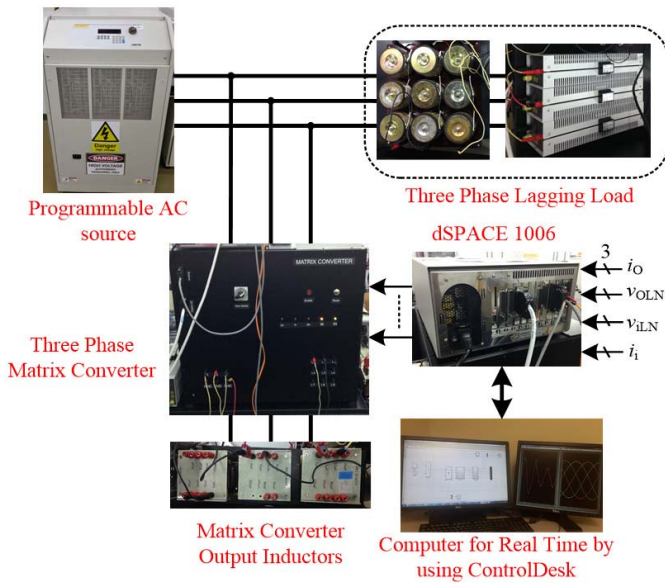


Fig. 7. Experimental setup of the proposed system.

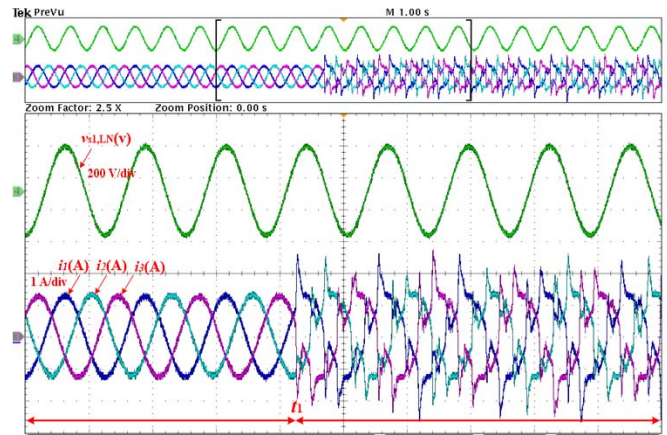


Fig. 8. Conventional MPC with fixed weight factor, model parameter error triggered at instant  $t_1$ : utility grid voltage ( $v_{s1,LN}$ ) and current ( $i_1$ ,  $i_2$ , and  $i_3$ ).

factor are shown in Fig. 13. The error to the model of the MC output-side inductance ( $L_{MC}$ ) from 30 to 15 mH is applied at time 0.06 s. As it is shown, without error in the inductance model, the proposed autotuned method has negligible reactive

power tracking error of less than 0.3%; however, the reactive power tracking error of the conventional fixed weight factor is 1.1%. The tracking performance improvement and robustness to system parameter error are shown after time 0.06 s, as it is shown that the proposed method has the tracking error of 1.04% with error in the inductance model which shows good disturbance rejection. However, the conventional fixed



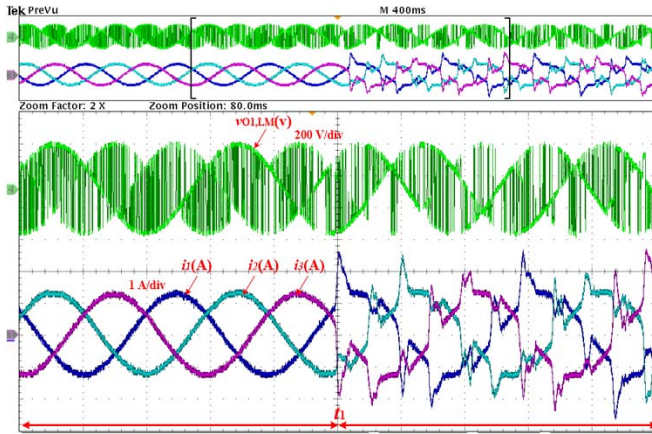


Fig. 9. Conventional MPC with fixed weight factor, model parameter error triggered at instant  $t_1$ : MC output voltage ( $v_{o1,LM}$ ) and current ( $i_1$ ,  $i_2$ , and  $i_3$ ).

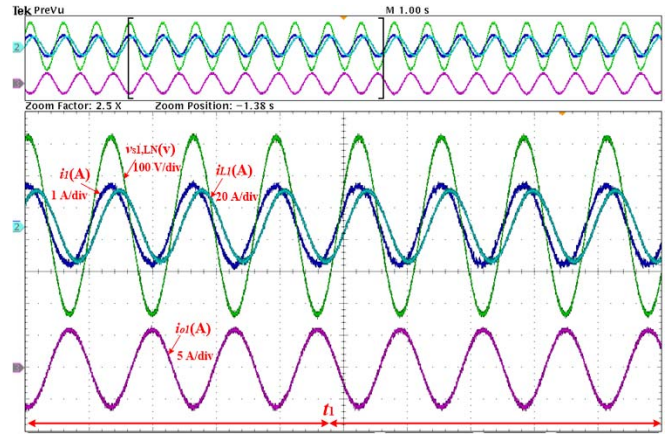


Fig. 12. Proposed MPC with autotuned weight factor, model parameter error triggered at instant  $t_1$ : utility grid voltage ( $v_{s1,LN}$ ), utility grid current ( $i_1$ ), MC output current ( $i_{o1}$ ), and load current ( $i_{L1}$ ).

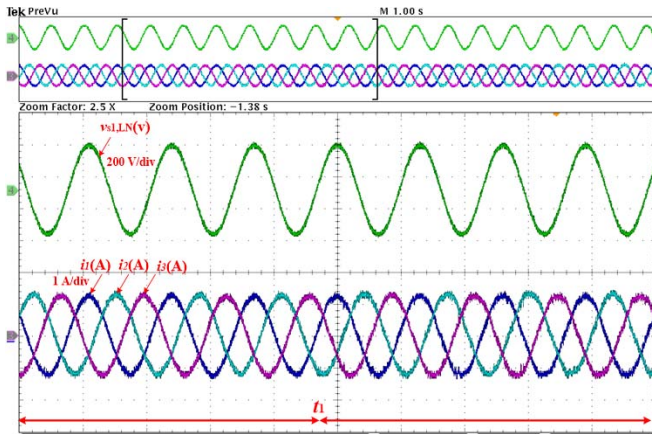


Fig. 10. Proposed MPC with autotuned weight factor, model parameter error triggered at instant  $t_1$ : utility grid voltage ( $v_{s1,LN}$ ) and current ( $i_1$ ,  $i_2$ , and  $i_3$ ).

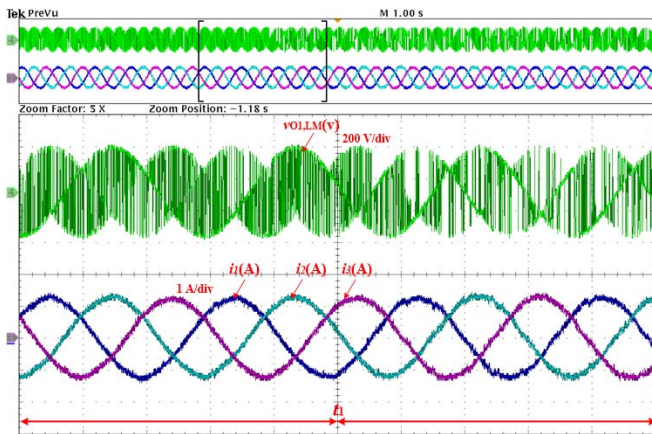
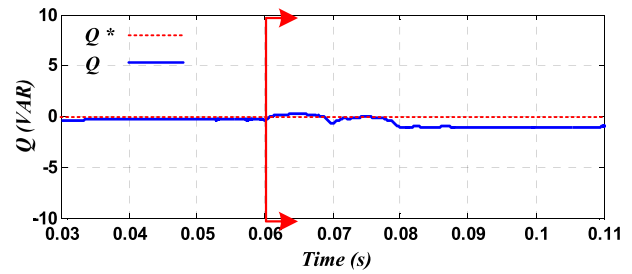
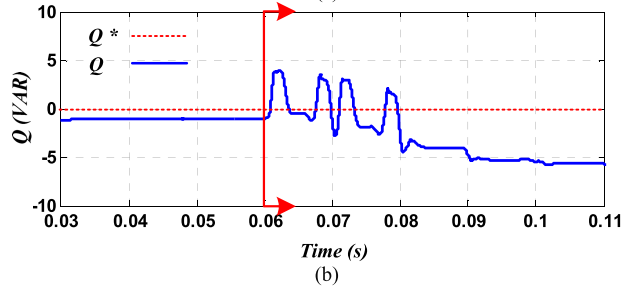


Fig. 11. Proposed MPC with autotuned weight factor, model parameter error triggered at instant  $t_1$ : MC output voltage ( $v_{o1,LM}$ ) and current ( $i_1$ ,  $i_2$ , and  $i_3$ ).



(a)



(b)

Fig. 13. Grid-side reactive power without and with errors in the inductance model after time 0.06 s. (a) Using the proposed autotuned cost function in MPC. (b) Using the conventional fixed weight factor.

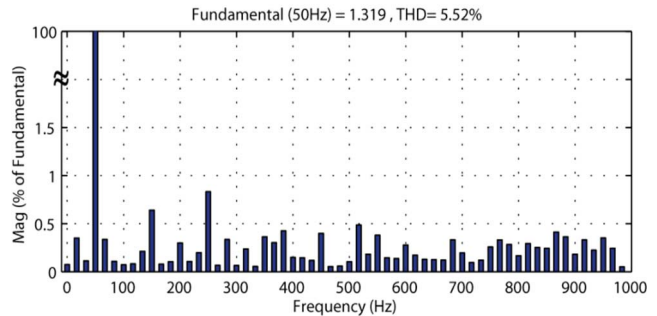


Fig. 14. Spectrum analysis of phase 1 of utility-side current ( $i_1$ ), without error in the inductance model at time 60 ms by using the conventional fixed weight factor.

weight factor method failed to track the zero reactive power (unity PF).

The spectrum analysis of phase 1 of the utility-side current ( $i_1$ ) without error in the inductance model from 30 to 15 mHz is illustrated in Fig. 14 by using the conventional fixed weight factor in the cost function, as it is shown that the THD is 5.52%. The spectrum analysis of phase 1 of the utility-side current ( $i_1$ ) without error in the inductance model by using

the proposed autotuned weight factor in the cost function is illustrated in Fig. 15, as it is depicted that the THD is dropped to 1.67%. By comparing Figs. 14 and 15, even without any disturbances in the models of the system, the proposed autotuned weight factor method significantly improves the

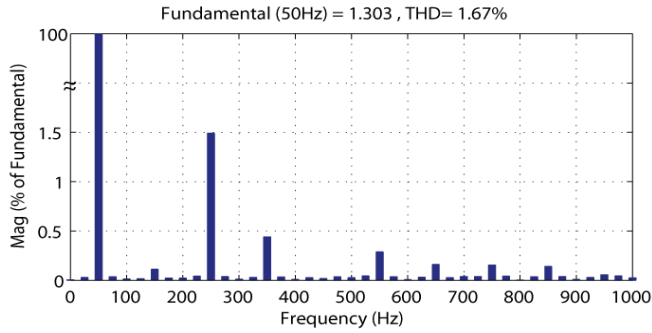


Fig. 15. Spectrum analysis of phase 1 of utility-side current ( $i_1$ ), without error in the inductance model at time 60 ms by using the proposed autotuned weight factor.

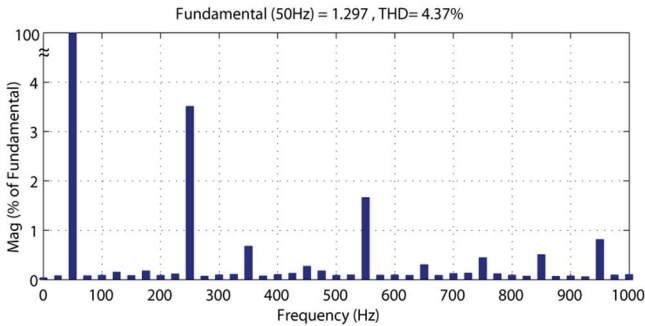
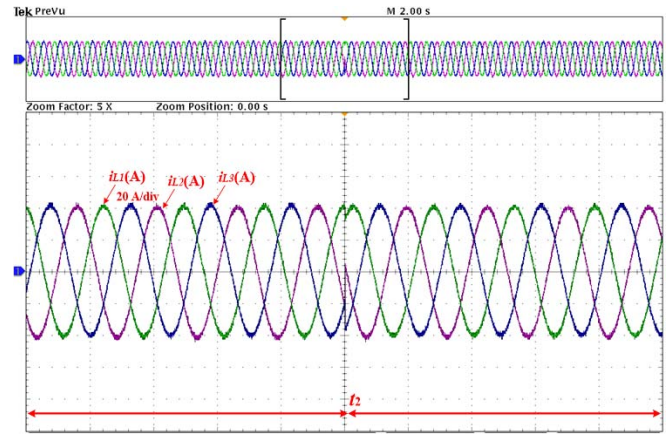


Fig. 16. Spectrum analysis of phase 1 of utility-side current ( $i_1$ ), after applying error in the inductance model at time 60 ms by using the proposed autotuned weight factor.

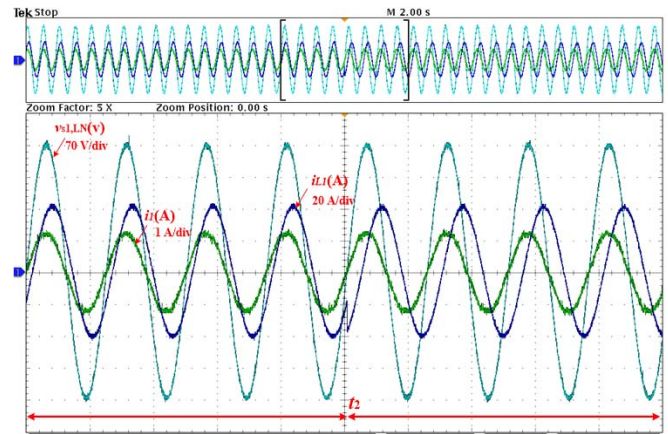
grid-side current quality. The spectrum analysis of phase 1 of the utility-side current is shown in Fig. 16 after applying error to the inductance model at time 0.06 ms. The THD is increased to 4.37% when using autotuned weight factor method, but still it meets the IEEE-519 [30], [31] standards limits. However, if the conventional fixed weight factor is used, the grid-side current will be highly distorted. Thus, the proposed autotuning weight factor technique overcomes one of the main limitations of MPC by improving the robustness of MPC to model parameter errors.

The PF step response on the utility side is shown in Fig. 17. The PF of the load has been stepped at instant  $t_2$  from 0.9 to 0.6. Fig. 17(a) shows the three-phase balanced load currents before and after the step changes in the load PF command at instant  $t_2$ . Fig. 17(b) shows utility current in the first phase and the load phase current in the first phase along with utility first-phase voltage to demonstrate the controller performance. As can be observed, the utility currents are providing the real part of the currents and are in phase with the utility voltage before and after the step responses in the load PF. The extra reactive power demand is supplied by the DMC.

Fig. 18 shows the effect of load unbalancing on the system. The load first-phase current ( $i_{L1}$ ) has been triggered at instant  $t_3$  to create an unbalanced condition on that load. Fig. 18(a) shows the utility voltage and currents for the first phase. The utility current in the first phase has been increased accordingly with respect to the load unbalance to cater the extra active demand in that phase. Fig. 18(b) shows the all phases of the load current.



(a)

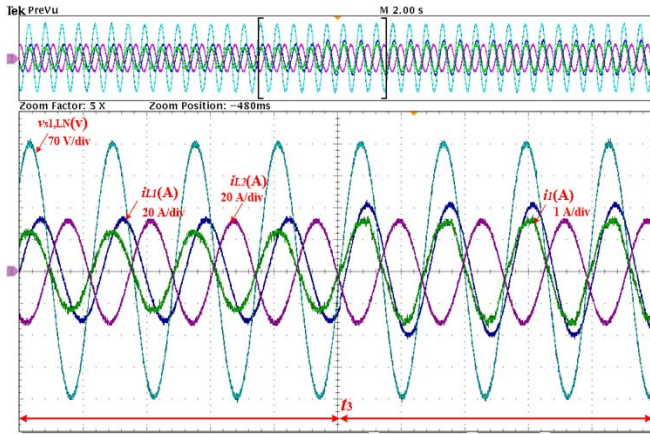


(b)

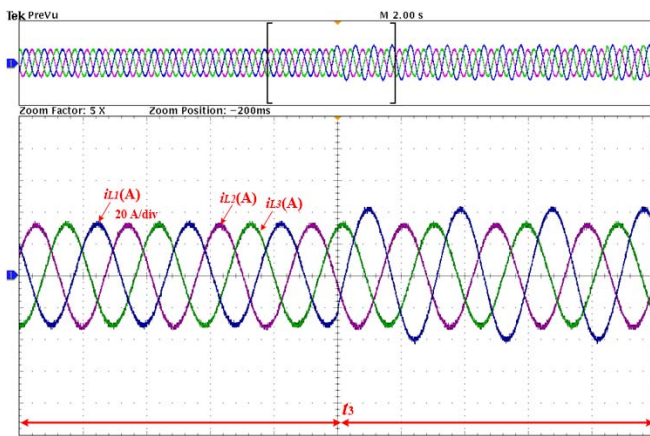
Fig. 17. Proposed MPC with autotuned weight factor, step change in load PF from 0.9 to 0.6 occurred at instant  $t_2$ . (a) Load current ( $i_{L1}$ ,  $i_{L2}$ , and  $i_{L3}$ ) with step change in PF. (b) Utility current ( $i_1$ ) and voltage ( $v_{o1,LM}$ ), and load current ( $i_{L1}$ ) before and after step changes in PF.

Finally, the voltage sag condition on the utility side has been analyzed and is shown in Fig. 19. A voltage sag at instant  $t_4$  has been introduced on the utility side. Load being the passive type; thus, the power requirement also comes down and can be observed in Fig. 19. The DMC-based STATCOM is still compensating the full reactive power of the load and maintaining the unity PF on the utility grid side.

In order to evaluate the computational burden of the proposed control scheme, its execution time has been measured. The required average time to perform all calculations is roughly  $50 \mu\text{s}$ . The sampling time is  $60 \mu\text{s}$ ; this sampling time is chosen based on the desired performance and complexity of the control scheme while considering the capability of the hardware microprocessor (dSPACE platform) we used for the system test. It turns out that the proposed control scheme uses approximately 85% of the available time. The execution time measurement shows that the implementation of the proposed control algorithm is feasible by most of the microcontrollers. The use of an embedded system like dSPACE is intended for expedited prototyping; however, when it comes to the real application and implementation, many cheaper boards like the Altera DEO-Nano field-programmable gate array that costs around U.S. \$85 is capable of handling the proposed controller.



(a)



(b)

Fig. 18. Proposed MPC with autotuned weight factor, unbalance load occurred at instant  $t_3$ . (a) Utility current ( $i_1$ ) and voltage ( $v_{o1,LM}$ ), and load current ( $i_{L1}$ ,  $i_{L2}$ ) before and after triggering the unbalance scenario. (b) Load current ( $i_{L1}$ ,  $i_{L2}$ , and  $i_{L3}$ ) before and after triggering the unbalance scenario.

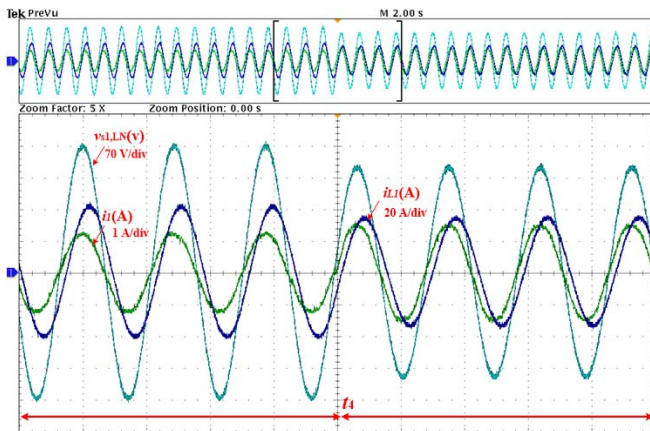


Fig. 19. Proposed MPC with autotuned weight factor, utility voltage sag of 40 V occurred at instant  $t_4$ .

## VI. CONCLUSION

The performance of MPC with multiple objectives in the cost function is directly affected by the weight factors. The proposed method in this paper determines the optimum weight factor of the cost function at each sampling time;

the optimization of the weight factor is done based on the prediction of objectives' absolute tracking error and their corresponding constraints. This technique eliminated the conventional trial-and-error approach to design the weight factor in the MPC cost function. Furthermore, the proposed approach improves the robustness of the model-based predictive control schemes to model parameter error.

Reactive power in the ac power system network while fundamental to the system is detrimental to the reliability, efficiency, and overall performance of the ac network. The application considered in this paper is a STATCOM by using the MPC of a DMC. MPC of the MC provides reactive power compensation by controlling the input reactive power and the output current into the inductive storage elements. The proposed autotuned technique for the MPC of the capacitor-less STATCOM by MC shows: lower THD at the grid-side current, robustness to the system model disturbances, and lower tracking error. Thus, the proposed control strategy and STATCOM are more reliable and robust technique for long service life of the device.

## REFERENCES

- [1] J. Holtz and S. Stadtfeld, "A predictive controller for the stator current vector of AC machines fed from a switched voltage source," in *Proc. Int. Power Electron. Conf. (IPEC)*, 1983, pp. 1665–1675.
- [2] J. Rodríguez and P. Cortes, *Predictive Control of Power Converters and Electrical Drives*. Hoboken, NJ, USA: Wiley, 2012.
- [3] J. Rodríguez *et al.*, "State of the art of finite control set model predictive control in power electronics," *IEEE Trans. Ind. Inform.*, vol. 9, no. 2, pp. 1003–1016, May 2013.
- [4] L. Tarisciotti, P. Zanchetta, A. Watson, P. Wheeler, J. C. Clare, and S. Bifaretti, "Multiobjective modulated model predictive control for a multilevel solid-state transformer," *IEEE Trans. Ind. Appl.*, vol. 51, no. 5, pp. 4051–4060, Sep./Oct. 2015.
- [5] J. Hu, J. Zhu, and D. G. Dorrell, "Model predictive control of grid-connected inverters for PV systems with flexible power regulation and switching frequency reduction," *IEEE Trans. Ind. Appl.*, vol. 51, no. 1, pp. 587–594, Jan./Feb. 2015.
- [6] L. Tarisciotti, P. Zanchetta, A. Watson, J. C. Clare, M. Degano, and S. Bifaretti, "Modulated model predictive control for a three-phase active rectifier," *IEEE Trans. Ind. Appl.*, vol. 51, no. 2, pp. 1610–1620, Mar./Apr. 2015.
- [7] A. Ayad, P. Karamanakos, and R. Kennel, "Direct model predictive current control strategy of quasi-Z-source inverters," *IEEE Trans. Power Electron.*, vol. 32, no. 7, pp. 5786–5801, Jul. 2016.
- [8] L. Wang *et al.*, "A finite control set model predictive control method for matrix converter with zero common-mode voltage," *IEEE J. Emerg. Sel. Topics Power Electron.*, vol. 6, no. 1, pp. 327–338, Mar. 2018.
- [9] P. Cortes *et al.*, "Guidelines for weighting factors design in model predictive control of power converters and drives," in *Proc. IEEE Int. Conf. Ind. Technol. (ICIT)*, Feb. 2009, pp. 1–7.
- [10] M. B. Shadmand, M. Mosa, R. S. Balog, and H. Abu-Rub, "Model predictive control of a capacitorless matrix converter-based STATCOM," *IEEE J. Emerg. Sel. Topics Power Electron.*, vol. 5, no. 2, pp. 796–808, Jun. 2017.
- [11] J. Garriga and M. Soroush, "Model predictive control tuning methods: A review," *Ind. Eng. Chem. Res.*, vol. 49, no. 8, pp. 3505–3515, 2010.
- [12] R. Shridhar and D. J. Cooper, "A tuning strategy for unconstrained multivariable model predictive control," *Ind. Eng. Chem. Res.*, vol. 37, no. 10, pp. 4003–4016, 1998.
- [13] W. Liu and G. Wang, "Auto-tuning procedure for model-based predictive controller," in *Proc. IEEE Int. Conf. Syst., Man, Cybern.*, vol. 5, Oct. 2000, pp. 3421–3426.
- [14] M. B. Shadmand, R. S. Balog, and H. Abu-Rub, "Model predictive control of a capacitor-less VAR compensator based on a matrix converter," in *Proc. IEEE Annu. Conf. Ind. Electron. Soc. (IECON)*, Oct./Nov. 2014, pp. 3311–3317.

- [15] S. R. Arya and B. Singh, "Performance of DSTATCOM using leaky LMS control algorithm," *IEEE J. Emerg. Sel. Topics Power Electron.*, vol. 1, no. 2, pp. 104–113, Jun. 2013.
- [16] Z. He *et al.*, "Reactive power strategy of cascaded delta-connected STATCOM under asymmetrical voltage conditions," *IEEE J. Emerg. Sel. Topics Power Electron.*, vol. 5, no. 2, pp. 784–795, Jun. 2017.
- [17] H. Wang *et al.*, "Transitioning to physics-of-failure as a reliability driver in power electronics," *IEEE J. Emerg. Sel. Topics Power Electron.*, vol. 2, no. 1, pp. 97–114, Mar. 2014.
- [18] B. Shi, B. Zhou, Y. Zhu, X. Qin, J. Lei, and N. Han, "Open-circuit fault analysis and diagnosis for indirect matrix converter," *IEEE J. Emerg. Sel. Topics Power Electron.*, vol. 6, no. 2, pp. 770–781, Jun. 2018.
- [19] S. Harb, H. Zhang, and R. S. Balog, "AC-link, single-phase, photovoltaic module integrated inverter," in *Proc. IEEE Appl. Power Electron. Conf. Expo. (APEC)*, Mar. 2013, pp. 177–182.
- [20] A. S. Farag *et al.*, "Failure analysis of composite dielectric of power capacitors used in distribution systems," in *Proc. Elect. Insul. Conf., Elect. Manuf. Coil Winding Conf.*, 1997, pp. 557–564.
- [21] W. Huai and F. Blaabjerg, "Reliability of capacitors for DC-link applications in power electronic converters: An overview," *IEEE Trans. Ind. Appl.*, vol. 50, no. 5, pp. 3569–3578, May 2014.
- [22] J. Bubic, R. Walling, K. O'Brien, and B. Kroposki, "The sun also rises," *IEEE Power Energy Mag.*, vol. 7, no. 3, pp. 45–54, May/June 2009.
- [23] M. Makdessi, A. Sari, P. Venet, P. Bevilacqua, and C. Joubert, "Accelerated ageing of metallized film capacitors under high ripple currents combined with a DC voltage," *IEEE Trans. Power Electron.*, vol. 30, no. 5, pp. 2435–2444, May 2015.
- [24] M. Arias, M. F. Diaz, D. G. Lamar, D. Balocco, A. A. Diallo, and J. Sebastián, "High-efficiency asymmetrical half-bridge converter without electrolytic capacitor for low-output-voltage AC–DC LED drivers," *IEEE Trans. Power Electron.*, vol. 28, no. 5, pp. 2539–2550, May 2013.
- [25] A. S. Farag *et al.*, "Failure analysis of composite dielectric of power capacitors in distribution systems," *IEEE Trans. Dielectr. Electr. Insul.*, vol. 5, no. 4, pp. 583–588, Aug. 1998.
- [26] A. M. Imam, D. M. Divan, R. G. Harley, and T. G. Habetler, "Real-time condition monitoring of the electrolytic capacitors for power electronics applications," in *Proc. IEEE Appl. Power Electron. Conf. (APEC)*, Feb./Mar. 2007, pp. 1057–1061.
- [27] P. Venet, H. Darnand, and G. Grellet, "Detection of faults of filter capacitors in a converter. Application to predictive maintenance," in *Proc. IEEE Telecommun. Energy Conf. (INTELEC)*, vol. 2, Sep. 1993, pp. 229–234.
- [28] A. Braham, A. Lahyani, P. Venet, and N. Rejeb, "Recent developments in fault detection and power loss estimation of electrolytic capacitors," *IEEE Trans. Power Electron.*, vol. 25, no. 1, pp. 33–43, Jan. 2010.
- [29] D. Balakrishnan and R. S. Balog, "Capacitor-less VAR compensator based on matrix converter," in *Proc. IEEE North Amer. Power Symp. (NAPS)*, Sep. 2010, pp. 1–7.
- [30] C. K. Duffey and R. P. Stratford, "Update of harmonic standard IEEE-519: IEEE recommended practices and requirements for harmonic control in electric power systems," *IEEE Trans. Ind. Appl.*, vol. 25, no. 6, pp. 1025–1034, Nov. 1989.
- [31] *IEEE Recommended Practice and Requirements for Harmonic Control in Electric Power Systems*, IEEE Standard 519-2014, IW Group, 1992.
- [32] H. Abu-Rub, J. Guzinski, Z. Krzeminski, and H. A. Toliyat, "Predictive current control of voltage-source inverters," *IEEE Trans. Ind. Electron.*, vol. 51, no. 3, pp. 585–593, Jun. 2004.
- [33] B. Arif, L. Tarisciotti, P. Zanchetta, J. C. Clare, and M. Degano, "Grid parameter estimation using model predictive direct power control," *IEEE Trans. Ind. Appl.*, vol. 51, no. 6, pp. 4614–4622, Nov./Dec. 2015.
- [34] T. Geyer, "A comparison of control and modulation schemes for medium-voltage drives: Emerging predictive control concepts versus PWM-based schemes," *IEEE Trans. Ind. Appl.*, vol. 47, no. 3, pp. 1380–1389, May/June 2011.
- [35] S. Mariethoz, A. Domahidi, and M. Morari, "High-bandwidth explicit model predictive control of electrical drives," *IEEE Trans. Ind. Appl.*, vol. 48, no. 6, pp. 1980–1992, Nov./Dec. 2012.
- [36] P. W. Wheeler, J. Rodríguez, J. C. Clare, L. Empringham, and A. Weinstein, "Matrix converters: A technology review," *IEEE Trans. Ind. Electron.*, vol. 49, no. 2, pp. 276–288, Apr. 2002.
- [37] J. Rodríguez, M. Rivera, J. W. Kolar, and P. W. Wheeler, "A review of control and modulation methods for matrix converters," *IEEE Trans. Ind. Electron.*, vol. 59, no. 1, pp. 58–70, Jan. 2012.
- [38] R. Vargas, J. Rodríguez, U. Ammann, and P. W. Wheeler, "Predictive current control of an induction machine fed by a matrix converter with reactive power control," *IEEE Trans. Ind. Electron.*, vol. 55, no. 12, pp. 4362–4371, Dec. 2008.
- [39] M. Rivera, J. Rodríguez, J. R. Espinoza, and H. Abu-Rub, "Instantaneous reactive power minimization and current control for an indirect matrix converter under a distorted AC supply," *IEEE Trans. Ind. Informat.*, vol. 8, no. 3, pp. 482–490, Aug. 2012.
- [40] F. Villarroel, J. R. Espinoza, C. A. Rojas, J. Rodríguez, M. Rivera, and D. Sbarbaro, "Multiobjective switching state selector for finite-states model predictive control based on fuzzy decision making in a matrix converter," *IEEE Trans. Ind. Electron.*, vol. 60, no. 2, pp. 589–599, Feb. 2012.



**Mohammad B. Shadmand** (S'09–M'15) received the B.S. degree in electrical engineering from Qatar University, Doha, Qatar, in 2010. He received the M.S. and Ph.D. degrees in electrical engineering from Texas A&M University, College Station, TX, USA, in 2012 and 2015, respectively.

From 2010 to 2015, he was a Research Associate with the Renewable Energy and Advanced Power Electronics Research Laboratory, Texas A&M University, College Station, TX, USA, where he was a TEES Research Engineer from 2016 to 2017.

In 2014, he joined the Smart Grid Center, Texas A&M University at Qatar, Doha, as a Visiting Researcher. From 2015 to 2016, he was an Instructor with the Department of Electrical and Computer Engineering, Texas A&M University. Since 2017, he has been an Assistant Professor with the Department of Electrical and Computer Engineering and the Director of the Renewable Energy and Power Quality Research Laboratory, Kansas State University, Manhattan, KS, USA. He has authored or co-authored over 50 journals and conference papers. His current research interests include advanced model predictive control, grid-tied power electronics interfaces with advance functionalities, matrix converter, and control of smart microgrid systems.

Dr. Shadmand was awarded second place in the IEEE Industrial Application Society Graduate Thesis Contest for his M.S. dissertation in 2013. He was a recipient of the IEEE Standard Education Award for the Project "fixed-step model predictive control of grid-tied photovoltaic inverter" in 2014 and the Michelle Munson\_serban Simu Keystone Research Scholar, Kansas State University, in 2017.



**Sarthak Jain** (S'13) received the B.Tech. degree in electrical engineering from Guru Gobind Singh Indraprastha University, New Delhi, India, in 2014. He is currently pursuing the master's degree in electrical engineering from Texas A&M University, College Station, TX, USA.

From 2016 to 2017, he was a Research Associate with the Renewable Energy and Advanced Power Electronics Laboratory, Texas A&M University. From 2014 to 2016, he was a Research Associate with Delhi Technological University, New Delhi.

He was with Imperial College London, London, U.K., and DST, New Delhi, with a focus on the project titled "Reliability and Efficient System for Community Energy Solutions." His current research interests include power electronic circuit design, dc/ac photovoltaic grid-tied inverters, and dc–dc resonant converters.



**Robert S. Balog** (S'92–M'96–SM'07) received the B.S. degree in electrical engineering from Rutgers—The State University of New Jersey, New Brunswick, NJ, USA, in 1996, and the M.S. and Ph.D. degrees in electrical engineering from the University of Illinois at Urbana–Champaign, Urbana, IL, USA, in 2003 and 2006, respectively.

From 1996 to 1999, he was an Engineer with Lutron Electronics, Coopersburg, PA, USA. From 2005 to 2006, he was a Researcher with the Construction Engineering Research Laboratory, Engineering Research and Development Center, U.S. Army Corps of Engineers, Champaign, IL, USA. From 2006 to 2009, he was a Senior Engineer with Sun-Power Inc., Champaign, IL, USA, and then he joined Texas A&M University, College Station, TX, USA, where he is currently an Associate Professor with

the Department of Electrical and Computer Engineering and the Director of the Renewable Energy and Advanced Power Electronics Research Laboratory. He is currently a Registered Professional Engineer in Illinois. He holds a joint faculty appointment with the Department of Electrical Engineering at Texas A&M University at Qatar, Doha, Qatar. He holds 14 issued U.S. patents with additional patents pending. His current research interests include power converters for solar energy, particularly microinverters for ac photovoltaic modules and highly reliable electrical power and energy systems including dc microgrids.

Dr. Balog is a member of Eta Kappa Nu, Sigma Xi, the National Society of Professional Engineers, the American Solar Energy Society, and the Solar Electric Power Association. He was a recipient of the Rutgers School of Engineering Distinguished Engineer Award in 2011 and the IEEE J. J. Suozzi INTELEC Fellowship in Power Electronics in 2001.